# Raspberry-like Metamolecules Exhibiting Strong Magnetic Resonances

Zhaoxia Qian,[†] Simon P. Hastings,[†,‡] Chen Li,[†] Brian Edward,[§] Christine K McGinn,[§] Nader Engheta,[‡,§] Zahra Fakhraai,[*,†] and So-Jung Park[*,†,‖]

[†]Department of Chemistry, [‡]Department of Physics, and [§]Department of Electrical and Systems Engineering, University of Pennsylvania, Philadelphia, Pennsylvania 19104, United States and [‖]Department of Chemistry & Nano Science, Ewha Womans University, 11-1, Daehyeon-dong, Seodaemun-gu, Seoul, South Korea

ABSTRACT We report a synthetic approach to produce raspberry-like plasmonic nanostructures with unusually strong magnetic resonances, termed raspberry-like metamolecules (raspberry-MMs). The synthesis based on the surfactant-assisted templated seed-growth method allows for the simultaneous one-step synthesis and assembly of well-insulated gold nanoparticles. The aromatic surfactant used for the syntheses forms a thin protective layer around the nanoparticles, preventing them from touching each other and making it possible to pack discrete nanoparticles at close distances
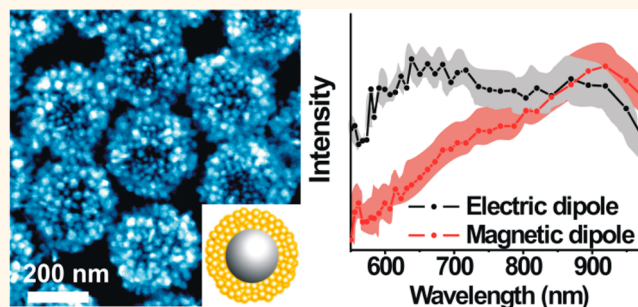
in a single cluster. The resulting isotropic gold nanoparticle clusters (*i.e.*, raspberry-MMs) exhibit unusually broad extinction spectra in the visible and near-IR region. Finite-difference time-domain (FDTD) modeling showed that the raspberry-MMs support strong magnetic resonances that contribute significantly to the broadband spectra. The strong magnetic scattering was also verified by far-field scattering measurements, which show that in the near-IR region the magnetic dipole resonance can be even stronger than the electric dipole resonance in these raspberry-MMs. Structural parameters such as the size and the number of gold nanoparticles composing raspberry-MMs can be readily tuned in our synthetic method. A series of syntheses with varying structure parameters, along with FDTD modeling and mode analyses of corresponding model structures, showed that the close packing of a large number of metal nanoparticles in raspberry-MMs is responsible for the unusually strong magnetic resonances observed here.

KEYWORDS: gold nanoparticle cluster · surface plasmon resonance · magnetic resonance · magnetic dipole · magnetic quadrupole · metamaterial · metamolecule

Coupling of the magnetic field of light with matter can enable unprecedented control and manipulation of light—matter interactions.[1,2] It has been proposed that subwavelength metal nanoparticles arranged into a two-dimensional ring structure or three-dimensional clusters can support magnetic resonances at optical frequencies.[3] This unusual property of metal nanoparticle clusters, which are often termed "metamolecules", has stimulated exciting new applications such as plasmonic cloaking,[4] superlenses,[5] and enhanced nonlinear optical properties.[6]

The majority of the effort in this area thus far has been focused on two-dimensional arrays fabricated by lithographic techniques[2] or by the assembly of presynthesized nanoparticles on solid substrates.[7−10] Compared to such two-dimensional structures,

three-dimensional clusters fabricated by solution chemistry are advantageous, as they can be produced in large quantities at low cost and are compatible with solution processing for the fabrication of metamaterials. In addition, isotropic metal nanoparticle clusters prepared by solution phase methods show orientation-independent optical and magnetic responses, which are difficult to achieve in lithographically fabricated structures. Recently, several approaches have been reported for three-dimensional clusters of metal nanoparticles showing magnetic resonances.[11−16] For example, Urban *et al.* reported the fabrication of three-dimensional gold nanoparticle clusters by the self-assembly of polystyrene-grafted gold nanospheres and an amphiphilic polymer, polystyrene-*block*-poly(acrylic acid) (PS-*b*-PAA).[15] In another example, Sheikholeslami *et al.* fabricated a
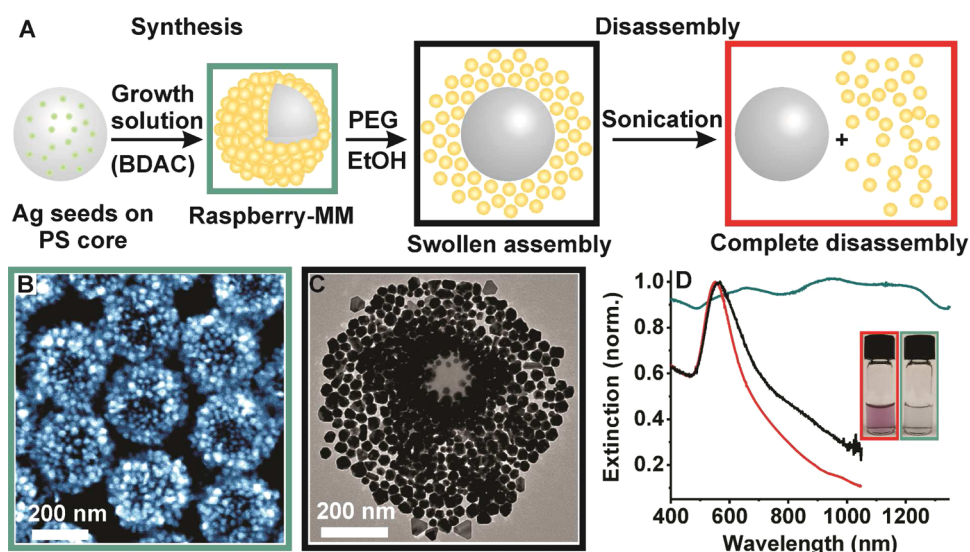
Figure 1. (A) Schematic description of the synthesis of raspberry-MMs by the templated surfactant-assisted seed-growth method and the disassembly procedure used to separate the Au nanobeads from the PS template. The large gray spheres, small blue spheres, and golden yellow spheres represent PS cores, silver seeds, and gold nanobeads, respectively. (B) SEM image of a typical raspberry-MM sample (MM_1) prepared with a PS template with the diameter of 184 ± 9 nm. Detailed synthetic conditions and size parameters are shown in Table 1. (C) Typical TEM images of the PEG-grafted raspberry-MMs redispersed in ethanol for 2 h. (D) UV−vis spectra of the raspberry-MMs shown in B (cyan), the swollen assemblies shown in C (black), and the disassembled nanoparticles obtained by 2 h sonication of the sample in C (red). See Figure S5 for the TEM image of disassembled nanoparticles. The inset is a picture of the raspberry-MM shown in B (right) and the dissembled structure after sonication (left).

shell-type metamolecule by assembling silver nanoparticles around a polystyrene (PS) core through streptavidin−biotin interactions.[13] The main challenge in realizing stronger magnetic resonances in such nanoparticle clusters is to further reduce the interparticle distance while simultaneously preventing the particles from contacting each other, which is difficult to achieve through typical self-assembly routes.

In this article, we report a new synthetic approach to prepare isotropic shell-type gold nanoparticle clusters exhibiting strong magnetic resonances. Our synthetic method, which is based on the templated surfactant-assisted seed-growth method, allows for *in situ* formation and assembly of gold nanobeads and yields raspberry-like structures where gold nanobeads are closely packed with only a few nanometers of separation (Figure 1A). The aromatic surfactant used in the synthesis acts as an effective dielectric coating on gold nanobeads and prevents them from contacting each other. The resulting nanoparticle clusters, which are termed here "raspberry-like metamolecules (raspberry-MMs)", showed unusually strong magnetic resonances, yielding broad extinction spectra in the visible and near-IR region. The strength of the magnetic dipole resonance in the raspberry-MMs increases with the size and the number of gold nanobeads in the assembly. Both experimental data and finite-difference time-domain (FDTD) simulations show that the magnetic dipole resonance can be even stronger than the electric dipole resonance in large raspberry-MMs. In addition, mode analyses revealed that the large raspberry-MMs

may also support magnetic quadrupole resonances, which has not been previously observed in other colloidal systems. These results demonstrate that the synthetic method described here provides an unparalleled ability to closely pack large numbers of well-insulated plasmonic nanobeads, which is the key requirement for the fabrication of metamolecules showing strong magnetic resonances in the visible and near-IR region.[3]

RESULTS AND DISCUSSION

Colloidal Synthesis and Characterization of Raspberry-MMs. The raspberry-MMs were synthesized by a templated surfactant-assisted seed-growth method as schematically described in Figure 1A. Briefly, a solution of PS cores decorated with silver seeds (seed solution) was mixed with a growth solution containing an aromatic surfactant, benzyl dimethyl hexadecyl ammonium chloride (BDAC), $HAuCl_4$, silver nitrate, and ascorbic acid (Figure 1A). This procedure is similar to our previously reported method used to produce spiky nanoshells[17,18] except that BDAC is used instead of cetyltrimethylammonium bromide (CTAB) as a surfactant. The synthetic method results in a raspberry-like structure composed of a PS core decorated with a large number of gold nanobeads (Figure 1B, Figures S1 and S2) in nearly 100% yield without any gold particles detached from PS cores. The gold nanobeads composing the raspberry-MMs maintained their discrete structure without fusing together. In comparison, nanoshells synthesized with alkyl surfactants such as cetyltrimethylammonium chloride

TABLE 1. Synthetic Conditions and Size Parameters of Raspberry-MMs Presented in Figures 1−5[a]

samples			experimental parameters				simulation parameters			
figure no.	sample no.	$V_{seed}/\mu L$	D_{core}/nm	N_{bead}	R_{bead}/nm	D_{RMM}/nm	D_{core}/nm	N_{bead}	R_{bead}/nm	D_{RMM}/nm
1B	MM_1	35	184 ± 9	>400	14.8 ± 5.0	337 ± 4	184	800[b]	14	340
2B	MM_2	70	94.5 ± 7.2	93 ± 10	11.8 ± 2.8	164 ± 14	96	100	12	161
2C	MM_3	50	94.5 ± 7.2	104 ± 21	13.8 ± 3.2	176 ± 14	96	100	13	175
2D	MM_4	35	94.5 ± 7.2	98 ± 10	16.3 ± 3.8	198 ± 14	96	100	16	195
2E	MM_5	20	94.5 ± 7.2	97 ± 15	19.4 ± 5.4	228 ± 23	96	100	19	230
3B	MM_6	35	56.4 ± 6.4	71 ± 6	15.4 ± 4.2	151 ± 13	56	70	11[c]	126
3D	MM_7	110	184 ± 9	>400	12.5 ± 2.1	290 ± 16	184	800[b]	11	287

[a] V_{seed}: volume of seed solution mixed with 10 mL of growth solution; D_{core}: diameter of PS core; R_{bead}: radius of Au nanobeads; N_{bead}: the number of Au nanobeads in each raspberry-MM; D_{RMM}: diameter of raspberry-MMs. Size parameters used in FDTD simulations are also given along with experimental parameters. [b] The number of beads used in the simulation was chosen to match the overall size of the actual raspberry-MMs with that of the model structure. [c] For MM_6, a smaller bead diameter was necessary to reproduce the experimental spectrum. This is probably due to the lower packing density of nanobeads in the experimental structure compared to the simulation model for raspberry-MMs synthesized on small-sized cores.

(CTAC) instead of BDAC formed fused nanoshells.[17] This result indicates that BDAC can form an efficient protecting layer on gold nanobeads.[19] Note that the key requirement in fabricating plasmonic three-dimensional metamolecules with strong magnetic resonances is to closely pack metal nanoparticles in a circular geometry without making contacts.[3] The discrete nature of gold nanobeads in the clusters synthesized here was further confirmed by replacing the BDAC coating with thiolated polyethylene glycol (PEG) (MW = 5000 g/mol) and then dispersing the raspberry-MMs in ethanol. This procedure increased the distance between gold nanobeads due to the swelling of PEG in ethanol as shown in Figure 1C and schematically depicted in Figure 1A (black box). The loosely bound nanobead network (Figure 1C) was then broken apart into individual nanobeads by sonication (Figure S5). This observation confirms that tightly packed gold nanobeads in the raspberry-MM are not in physical contact, as they are well-protected by the BDAC layers. In addition, this disassembly procedure allowed us to analyze the size, number, and shape of the beads in great detail. The beads were predominantly spherical or quasi-spherical in shape with a few triangular and rod-like structures (Figure 1C). The structural parameters obtained from the measurements are listed in Table 1.

The raspberry-MMs exhibited broadband extinction spectra covering from 500 nm to over 1200 nm with distinct resonance peaks at 658, 943, and 1222 nm (Figure 1D, cyan). The disassembled Au beads, on the other hand, showed an SPR band at 552 nm (Figure 1D, red), which is slightly red-shifted compared to the SPR band position (526 nm) of isolated spherical nanoparticles of similar size in ethanol.[20,21] This slight red-shift and the tail in the longer wavelength region (Figure 1D, red) are probably due to some remaining small clusters of gold nanobeads.[22] Nonetheless, the extinction spectra and TEM measurements as well as the red color of the disassembled sample (Figure 1D, inset) confirm that most Au beads maintain well-isolated structures in

raspberry-MMs. It is also important to note that PEG-modified raspberry-MMs incubated in ethanol (Figure 1C) showed an extinction spectrum (Figure 1D, black) close to that of isolated gold nanobeads (Figure 1D, red), indicating that the short interparticle distance in raspberry-MMs is an important contributing factor to the broad extinction spectrum of raspberry-MMs (Figure 1D, cyan).

Optical Properties of Raspberry-MMs with Varying Structural Parameters. It is well known that the optical properties of metallic nanoparticle clusters are strongly dependent on the size and the number of particles composing the clusters as well as interparticle distance.[22,23] In the synthetic method presented here, those parameters can be readily controlled. Figure 2 presents SEM images and extinction spectra of a series of raspberry-MMs composed of different sized Au beads fabricated on 94.5 nm PS cores (see Figure S3 for TEM images). The average number of beads was kept constant at about 100 (Figure S6) for all four samples (Table 1). The radius of the beads was increased from 11.8 ± 2.8 nm to 19.4 ± 5.4 nm by adjusting the volume ratio between the seed and the growth solution (V_{seed}/V_{growth}) (Figure 2). All four clusters showed broadband extinction spectra (Figure 2F, top) composed of mainly two peaks, covering the visible and near-IR region. The long-wavelength peak red-shifted and the overall bandwidth became broader with increasing Au bead sizes.

Finite-difference time-domain modeling (Lumerical Solutions, Inc.) was carried out to investigate the broad profile of the extinction spectra (Figure 2F, bottom). To generate realistic models of raspberry-MMs, a separate molecular dynamics simulation was used to randomly pack Au beads on the surface of a PS template (see Supporting Information section I for more details). Structural parameters such as the number of gold nanobeads, the size of gold nanobeads, and the PS core diameter were chosen based on experimental values (Table 1). All models were constructed with Au spheres coated with a 1 nm thick dielectric (Figure 2G), which generated nanoparticle clusters with the average nearest
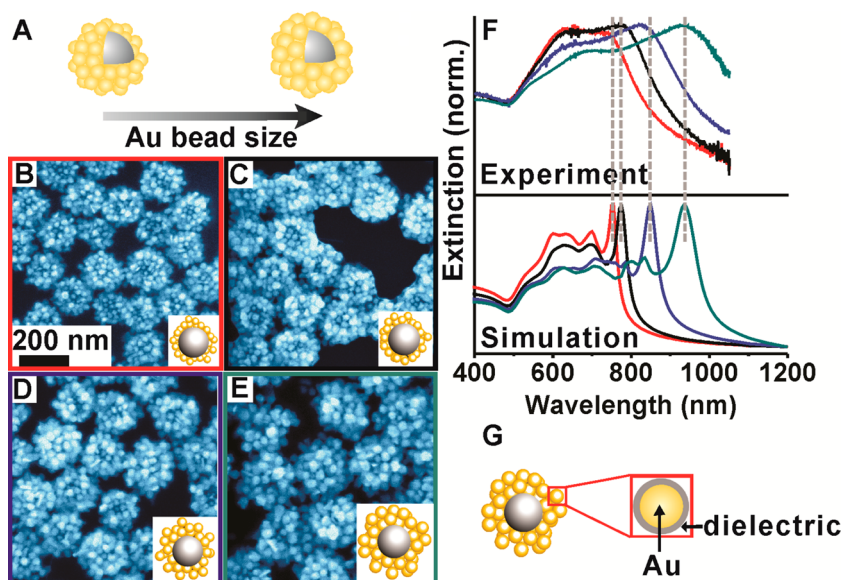
Figure 2. Raspberry-MMs composed of different sized Au beads. (A–E) Schematic description (A) and SEM images (B–E) of raspberry-MMs with increasing bead size. The insets in B–D show the cross sections of corresponding models used in simulations. (G) Model for the cluster shown in D used in FDTD simulations. (F) Experimental (top) and simulated (bottom) extinction spectra of samples in B (MM_2 (D_{core} = 96 nm, N_{bead} = 100, R_{bead} = 12 nm), red), C (MM_3 (D_{core} = 96 nm, N_{bead} = 100, R_{bead} = 13 nm), black), D (MM_4 (D_{core} = 96 nm, N_{bead} = 100, R_{bead} = 16 nm), blue), and E (MM_5 (D_{core} = 96 nm, N_{bead} = 100, R_{bead} = 19 nm), cyan). The synthetic conditions and structural parameters are summarized in Table 1.

neighbor bead-to-bead distance of about 2.0 nm (Figure S9); this is a reasonable number considering the thickness of the BDAC layer (Figure S10). The coordinates of each nanobead obtained from the molecular dynamics simulation were then imported into the Lumercial software (Lumerical Solutions, Inc.) for FDTD modeling. The details of the FDTD modeling have been reported in our earlier publications.[17,18] Extensive tests were carried out to make sure that the simulated results converge (Supporting Information, Figures S11, S12).

The spectroscopic features and major peak positions of simulated spectra (Figure 2F, bottom, Figure S13) exhibit similar profiles and trends to those of experimental spectra (Figure 2F, top), although fine features of sharp peaks in the simulated single-particle spectra are smoothed and broadened in the experimental ensemble spectra. Because each raspberry-MM should have slightly different structural parameters (e.g., the number of beads, the size of beads, bead arrangements, interbead distances), the experimental ensemble spectra are broader than the simulated spectra (Figure S14). Nonetheless, the general agreement between the simulation and the experimental peak positions (as guided by the gray dashed lines) indicates that the structural parameters used for these simulations are appropriate and that the optical properties of raspberry-MMs can be effectively controlled by varying the size of Au beads.

The optical properties of raspberry-MMs can also be tuned by varying the core diameter. Figure 3 shows the structure and extinction spectra of three different raspberry-MMs prepared with different sized PS cores

(56.4, 94.5, and 184 nm in diameter) (see Figure S4 for TEM images). The radius of Au beads in the three clusters was kept constant at about 13.2 nm (Table 1) by carefully adjusting V_{seed}/V_{growth}. The average numbers of Au nanobeads on the 56.4 and 94.5 nm diameter PS core counted from TEM images were 71 ± 6 and 93 ± 10, respectively (Table 1, Figures S6, S7). The average number of Au beads on the 184 nm core was estimated to be around 800 from the overall size of the cluster, as it was difficult to accurately count the large number of beads for the structure due to the overlap of beads around the PS core (Figure S8). The structure parameters for the assemblies are provided in Table 1.

The smallest raspberry-MMs exhibited a major peak at 629 nm and a shoulder at 740 nm (Figure 3E, top, black). The medium-sized raspberry-MMs showed similar spectral features, but the long-wavelength peak slightly red-shifted to 743 nm, and its intensity increased and became comparable to that of the 629 nm peak (Figure 3E, top, red). In the largest raspberry-MMs, the spectrum became much broader with three major peaks (Figure 3E, top, blue). In general, the extinction spectra of the raspberry-MMs became broader and extended further into the near-IR region with increasing overall size of the assemblies (Figure 3E, top).

The calculated spectrum of the small raspberry-MM model (MM_6) shows a main peak at 595 nm and weaker peaks on the long-wavelength shoulder, which drops quickly at 733 nm (Figure 3E (bottom, black), Figure S15). The simulated spectrum of the medium-sized raspberry-MM (MM_2) exhibits similar features to
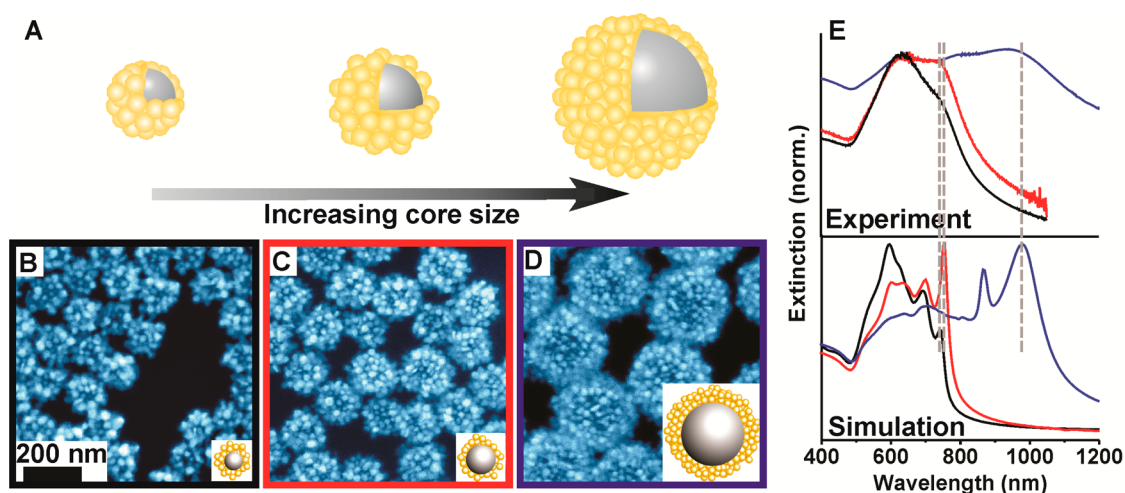
Figure 3. Raspberry-MMs formed with different sized cores. (A−D) Schematic description (A) and SEM images (B−D) of raspberry-MMs formed with different-sized cores (B: MM_6 (D_{core} = 56 nm, N_{bead} = 70, R_{bead} = 11 nm), C: MM_2 (D_{core} = 96 nm, N_{bead} = 100, R_{bead} = 12 nm), D: MM_7 (D_{core} = 184 nm, N_{bead} = 800, R_{bead} = 11 nm)). The insets in B−D show the cross sections of corresponding models used in the simulation. Detailed structural parameters are given in Table 1 along with the synthetic condition. (E) Experimental (top) and simulated (bottom) extinction spectra of samples in B (black), C (red), and D (blue).

that of the small raspberry-MM, but the long-wavelength peak shows a slight red-shift and significantly increased intensity (Figure 3E, bottom, red). This spectral trend is consistent with the experimental results as indicated with gray dashed lines (Figure 3E, top). The simulated spectrum for the large raspberry-MM (MM_7) exhibits further red-shifts and spectral broadening (Figure 3E (bottom, blue), Figure S15), again consistent with the trend observed in the experimental spectra (Figure 3E, top). In general, the main features and trends in the simulated spectra (Figure 3E, bottom) agree fairly well with the experimental spectra (Figure 3E, top), with both simulation and experimental data showing red-shifts and spectral broadening with increasing sizes of the assemblies.

Mode Analyses. In order to understand the origin of the unusually broadband extinction of raspberry-MMs, the scattering, absorption, and extinction cross sections were calculated (Figure 4A) for a model raspberry-MM shown in Figure 1B, and the scattered field was resolved into the contributions of different electric and magnetic modes[24] (Figure 4B; see Supporting Information for more details). The peak positions of the calculated extinction spectrum (Figure 4A, blue) are consistent with those of the experimental spectrum (Figure 4A, cyan), covering a broad spectral range from 500 nm to over 1200 nm with a somewhat higher intensity in the near-IR region than that in the visible region. The extinction between 500 and 878 nm arises from both absorption and scattering, while scattering dominates the spectrum at wavelengths longer than 878 nm (Figure 4A).

The scattering cross section of a large raspberry-MM was decomposed into individual multipole components by projecting the FDTD-generated scattered field onto a vector spherical harmonic expansion
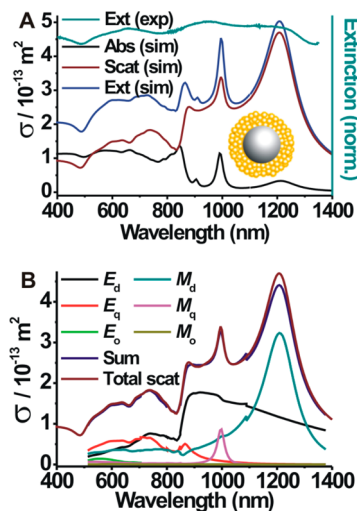
Figure 4. Mode analyses of the extinction spectrum for a raspberry-MM. (A) Absorption, scattering, and extinction cross sections of a modeled raspberry-MM calculated with experimentally obtained geometric parameters for raspberry-MMs shown in Figure 1B (MM_1: D_{core} = 184 nm, N_{bead} = 800, R_{bead} = 14 nm). The experimental extinction spectrum is shown in cyan for comparison. The inset shows the cross section of the simulation model. (B) Calculated scattering cross section (σ) of different electric and magnetic modes and their sum (E_d: electric dipole, E_q: electric quadrupole, E_o: electric octopole, M_d: magnetic dipole, M_q: magnetic quadrupole, M_o: magnetic octopole, Sum: sum of the cross sections of all six calculated electric and magnetic modes). The total scattering spectrum directly obtained by FDTD simulation (labeled as Total scat) is also presented for comparison.

(see Supporting Information for details). Figure 4B presents the calculated scattering cross section for the electric dipole, electric quadruple, electric octopole, magnetic dipole, magnetic quadrupole, and magnetic octopole as well as the sum of the six spectra. The sum of the component multipoles (Figure 4B, navy) matches well with the total scattering spectrum calculated using

FDTD (Figure 4B, brown), demonstrating that these modes are enough to describe the far-field behavior.

The data presented in Figure 4B shows that the electric dipole and electric quadrupole modes are quite broad without distinct resonance peaks. This is due to the fact that the structure is fairly heterogeneous and the nanobeads are not in contact with each other.[17] In a previous study, we have shown that when gold nanoparticles decorating a polymer core touch to form a full shell, the electric dipole resonance becomes strong and sharp.[17] In the raspberry-MMs, where gold nanobeads on a PS core are not in contact, the electric dipole (Figure 4B, black) and electric quadrupole (Figure 4B, red) scattering spectra predominantly originate from many local dipolar oscillations on the single-particle level and their interactions with each other. In contrast, distinct and strong resonances are observed in the magnetic dipole (Figure 4B, cyan) and the magnetic quadrupole (Figure 4B, magenta) scattering spectra. The magnetic dipole resonance makes a significant contribution to the longest wavelength scattering peak at 1207 nm (Figure 4B, cyan). Significantly, the contribution of magnetic dipole resonance to the scattering at this wavelength is even higher than that of the electric dipole scattering (Figure 4B). Furthermore, a distinct magnetic quadrupole resonance is observed at 995 nm (Figure 4B, magenta). The intensity of higher order modes such as the electric octopole and the magnetic octopole is much weaker than that of the lower order modes, confirming that the dipole and quadruple modes dominate the scattering spectrum. The sum of all six modes is in excellent agreement with the total simulated scattering cross section, indicating that mode mixing is also negligible in the total scattering cross section of these structures.

Measurements of Electric and Magnetic Dipole Scattering. The existence of strong magnetic dipole scattering of these raspberry-MMs was also experimentally confirmed by measuring the electric dipole and magnetic dipole scattering spectra of these particles at 90° scattering angle and at the polarization angles indicated in Figure 5A (see Supporting Information for detailed experimental setup (Scheme S1)). The data collected for MM_1 (D_{core} = 184 nm, N_{bead} = 800, R_{bead} = 14 nm) are presented in Figure 5B. Additional experimental data for other raspberry-MMs as well as control experiments on smooth nanoshells and nanospheres are shown in Figure S16 (extinction spectra) and Figure S17 (scattering at 90° angle) in the Supporting Information.

Significantly, the experimental data presented in Figure 5B show strong magnetic dipole scattering that exceeds the scattering from the electric dipole in the near-IR region. The magnetic and electric scattering spectra for 90° angle data collection were calculated for the MM_1 model and presented in Figure 5C for comparison. The calculated scattering spectra show
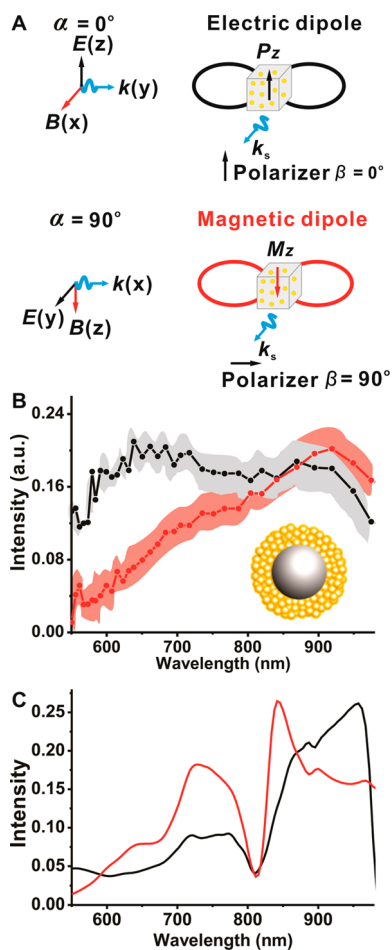
Figure 5. Experimental measurements for the scattering from the electric and magnetic dipoles induced in MM_1 (D_{core} = 184 nm, N_{bead} = 800, R_{bead} = 14 nm). (A) Schematic description of the measurement setup, showing the electric field, magnetic field, and the propagation directions of the incident polarized laser beam. The polarization direction of the incident and scattering electric field is indicated with α and β, respectively. The top figure (α = 0°, β = 0°) shows the geometry that leads to the electric dipole scattering measurements, and the bottom figure (α = 90°, β = 90°) shows the geometry required to measure the magnetic dipole scattering. The gray box with golden yellow dots schematically represents a raspberry-MM solution in a cuvette used for the measurement. (B) Measured scattering intensity from the electric dipole (black curve) and magnetic dipole (red curve) at described polarization directions. The gray area and red area represent the possible errors due to background processes such as multiple scattering. These errors are measured by the cross-polarization configuration (α = 0°, β = 90° for the electric dipole and α = 90°, β = 0° for the magnetic dipole). (C) Calculated scattering intensity from the electric dipole (black curve) and magnetic dipole (red curve) of the model raspberry-MM at the scattering angle of 90° with respect to the incident plane wave light source.

complicated spectral features with signs of interference. Much of the detailed spectral features in the calculated spectra (Figure 5C) are washed out in the experimental spectra (Figure 5B) due to the heterogeneity in the experimental structure and the ensemble averaging effect. Single-particle scattering measurements are required to accurately correlate the experimental and calculated spectra and to understand the origins of the

interesting interference patterns. Effort in this direction is under way. Nonetheless, it is clear that both the calculated and experimental spectra show strong magnetic resonances with intensities comparable to or exceeding those of electric resonances. Indeed, the data presented in Figure 5B confirm that the magnetic resonance modes make significant contributions to the far-field scattering in the near-IR and the broad extinction of raspberry-MM. The measured scattering intensity for the magnetic dipole already exceeds that of the electric dipole at wavelengths over 850 nm (Figure 5B). Since the magnetic dipole peak is located at 1200 nm in the simulated spectra (Figure 4, Figure S18), the magnetic dipole scattering at that wavelength should be even stronger than the maximum value found in the range measured in this study.

Origins of the Magnetic Dipole and Quadrupole Modes. For a nonmagnetic material, magnetic resonances can be created by resonating loops of displacement current.[3] This can be achieved in closely packed subwavelength metallic nanoparticles.[3] The boundary conditions at the surfaces of the nanoparticle dictate that the direction of the electric field should always be normal to the surface of the particle. Therefore, in circularly arranged nanoparticles, at each boundary the electric field rotates slightly, leading to a full circulation of the light's electric field at a resonance around the raspberry-MMs. This results in circularly rotating polarization currents that generate a magnetic field normal to the plane of the nanoparticle cluster.[25,26] This phenomenon supports magnetic dipole resonances in the raspberry-MMs studied here. While the PS core in raspberry-MMs does not significantly affect the optical responses of raspberry-MMs (Figure S19), the spherical shape of the core allows for the fabrication of isotropic clusters of nanoparticles exhibiting angle-independent optical responses (Figure S20).

The experimental and simulation results presented in Figures 2 and 3 show that the magnetic resonances become stronger as the cluster size becomes larger (Figure S21, Figure 4B), consistent with previous reports.[14,27] The size of nanoparticle clusters can be readily controlled in our synthesis method, as demonstrated in Figures 2 and 3, allowing for the control of

the strength and peak positions of magnetic resonances. While magnetic dipole resonances have been previously observed in other nanoparticle clusters,[9,10] the raspberry-type assemblies studied here show unprecedentedly strong magnetic dipole resonances due to the small interparticle distances as well as the large cluster size.

Magnetic quadrupole resonances in nanoparticle clusters can be potentially generated by multiple loops of current that are separated enough to generate a phase difference between them.[28] Note that the cross section of a magnetic quadrupole mode is typically very weak, and it is challenging to fabricate nanoparticle clusters that can support magnetic quadrupole modes by self-assembly routes. In our synthetic approach, multiple layers of gold nanoparticles can be readily assembled on a PS core, where multiple closed current loops can be generated with the necessary phase lag to support magnetic quadrupole resonances.

CONCLUSIONS

In summary, we developed a synthetic approach to construct tightly packed isotropic raspberry-like metamolecules exhibiting strong magnetic resonances. The synthetic method presented here simplifies the fabrication process, as it allows for one-pot *in situ* synthesis and assembly of nanoparticles, where various structural parameters such as the size and the number of Au beads can be readily controlled. The aromatic surfactant used here, BDAC, forms a protective layer around the nanobeads, keeping the distance between them within a few nanometers and maintaining their discrete nature in the clusters. This method generates well-defined clusters of tightly packed, well-insulated nanoparticles with controlled aggregation number (*i.e.*, size of clusters), leading to unprecedentedly strong magnetic dipole resonances at optical frequencies, as is verified both experimentally and *via* FDTD simulations. The robustness and tunability of the synthetic method presented here and the strong magnetic responses of resulting nanoparticle clusters can lead to large-scale manufacturing and wide applications of magnetic metamaterials.

METHODS

Syntheses of Raspberry-like Metamolecules. Isotropic raspberry-like metamolecules (raspberry-MMs) were synthesized by a modified surfactant-assisted templated seed growth method.[17,18,29] Carboxylate-modified FluoSpheres (diameter: 60 nm, 100 nm, 200 nm, 4 wt % solids for 60 nm fluospheres, 2% wt solids for 100 and 200 nm fluospheres, 100 μL) were mixed with an aqueous solution of Ag(NH$_3$)$_2$$^+$ (0.01 M, 100 μL) for 30 min. Then the mixture was washed by centrifugation at 16 000 rpm for 30 min and redispersed in nanopure water. The same washing procedure was repeated one more time, and the precipitates were redispersed in 500 μL of water. Then an aqueous solution of freshly prepared NaBH$_4$ (0.01 M, 100 μL) was added to the

solution with vigorous mixing. The seed solution was aged overnight and then centrifuged at 16 000 rpm for 30 min. The precipitates were then redispersed in 5 mL of water.

Typical growth solution was prepared by mixing aqueous solutions of BDAC (0.1 M, 10 mL), HAuCl$_4$ (0.01 M, 421 μL), AgNO$_3$ (0.01 M, 64 μL), and ascorbic acid (0.1 M, 67 μL), sequentially. Varying amounts of seed solution (35 to 110 μL, exact amount for each sample was provided in the main text) were added to the growth solution (10 mL) followed by gentle mixing (a few seconds). A bluish-green color started to develop after approximately 10 min, and the reaction was completed in about 2 h.

In order to examine the internal structure, synthesized raspberry-MMs were washed once by centrifugation at

3000 rpm for 10 min and then resuspended in a 0.8 mg/mL thiolated-polyethylene glycol (PEG5000, Sigma-Aldrich) aqueous solution and kept in the solution overnight. The solution was then centrifuged to remove excess PEG, and the PEG-modified raspberry-MMs were redispersed and kept in ethanol for at least 4 h before sonication.

Characterization of Raspberry-MMs. Transmission electron microscope (TEM) images were taken with a JEOL TEM-2010 at an accelerating voltage of 200 kV. Energy-dispersive X-ray spectroscopy (EDX) measurements were carried out using a JEOL 2010F at an accelerating voltage of 200 kV. Scanning electron microscope (SEM) images were taken with a Quanta 600 FEG Mark II SEM at an accelerating voltage of 30 kV. An Agilent 8453 UV−visible spectrophotometer was used for extinction spectra.

Conflict of Interest: The authors declare no competing financial interest.

Supporting Information Available: Detailed experimental and simulation methods, additional TEM images, and FDTD simulations. This material is available free of charge *via* the Internet at http://pubs.acs.org.

REFERENCES AND NOTES

1. Pendry, J. B.; Holden, A. J.; Robbins, D. J.; Stewart, W. J. Magnetism from Conductors and Enhanced Nonlinear Phenomena. *IEEE Trans. Microwave Theory Tech.* **1999**, *47*, 2075–2084.

2. Soukoulis, C. M.; Wegener, M. Past Achievements and Future Challenges in the Development of Three-Dimensional Photonic Metamaterials. *Nat. Photonics* **2011**, *5*, 523–530.

3. Alù, A.; Engheta, N. The Quest for Magnetic Plasmons at Optical Frequencies. *Opt. Express* **2009**, *17*, 5723–5730.

4. Chen, P.-Y.; Soric, J.; Alù, A. Invisibility and Cloaking Based on Scattering Cancellation. *Adv. Mater.* **2012**, *24*, 281–304.

5. Casse, B. D. F.; Lu, W. T.; Huang, Y. J.; Gultepe, E.; Menon, L.; Sridhar, S. Super-Resolution Imaging Using a Three-Dimensional Metamaterials Nanolens. *Appl. Phys. Lett.* **2010**, *96*, 023114.

6. Argyropoulos, C.; Chen, P.-Y.; Monticone, F.; D'Aguanno, G.; Alù, A. Nonlinear Plasmonic Cloaks to Realize Giant All-Optical Scattering Switching. *Phys. Rev. Lett.* **2012**, *108*, 263905.

7. Fan, J. A.; Wu, C.; Bao, K.; Bao, J.; Bardhan, R.; Halas, N. J.; Manoharan, V. N.; Nordlander, P.; Shvets, G.; Capasso, F. Self-Assembled Plasmonic Nanoparticle Clusters. *Science* **2010**, *328*, 1135–1138.

8. Yap, F. L.; Thoniyot, P.; Krishnan, S.; Krishnamoorthy, S. Nanoparticle Cluster Arrays for High-Performance SERS through Directed Self-Assembly on Flat Substrates and on Optical Fibers. *ACS Nano* **2012**, *6*, 2056–2070.

9. Shafiei, F.; Monticone, F.; Le, K. Q.; Liu, X.-X.; Hartsfield, T.; Alu, A.; Li, X. A Subwavelength Plasmonic Metamolecule Exhibiting Magnetic-Based Optical Fano Resonance. *Nat. Nanotechnol.* **2013**, *8*, 95–99.

10. Barrow, S. J.; Wei, X.; Baldauf, J. S.; Funston, A. M.; Mulvaney, P. The Surface Plasmon Modes of Self-Assembled Gold Nanocrystals. *Nat. Commun.* **2012**, *3*, 1275.

11. Lim, S.; Song, J. E.; La, J. A.; Cho, E. C. Gold Nanospheres Assembled on Hydrogel Colloids Display a Wide Range of Thermoreversible Changes in Optical Bandwidth for Various Plasmonic-Based Color Switches. *Chem. Mater.* **2014**, *26*, 3272–3279.

12. Larson-Smith, K.; Pozzo, D. C. Scalable Synthesis of Self-Assembling Nanoparticle Clusters Based on Controlled Steric Interactions. *Soft Matter* **2011**, *7*, 5339–5347.

13. Sheikholeslami, S. N.; Alaeian, H.; Koh, A. L.; Dionne, J. A. A Metafluid Exhibiting Strong Optical Magnetism. *Nano Lett.* **2013**, *13*, 4137–4141.

14. Muhlig, S.; Cunningham, A.; Scheeler, S.; Pacholski, C.; Burgi, T.; Rockstuhl, C.; Lederer, F. Self-Assembled Plasmonic Core-Shell Clusters with an Isotropic Magnetic Dipole Response in the Visible Range. *ACS Nano* **2011**, *5*, 6586–6592.

15. Urban, A. S.; Shen, X.; Wang, Y.; Large, N.; Wang, H.; Knight, M. W.; Nordlander, P.; Chen, H.; Halas, N. J. Three-Dimensional Plasmonic Nanoclusters. *Nano Lett.* **2013**, *13*, 4399–4403.

16. Pazos-Perez, N.; Wagner, C. S.; Romo-Herrera, J. M.; Liz-Marzán, L. M.; García de Abajo, F. J.; Wittemann, A.; Fery, A.; Alvarez-Puebla, R. A. Organized Plasmonic Clusters with High Coordination Number and Extraordinary Enhancement in Surface-Enhanced Raman Scattering (SERS). *Angew. Chem., Int. Ed.* **2012**, *51*, 12688–12693.

17. Sanchez-Gaytan, B. L.; Qian, Z.; Hastings, S. P.; Reca, M. L.; Fakhraai, Z.; Park, S.-J. Controlling the Topography and Surface Plasmon Resonance of Gold Nanoshells through Templated Surfactant-Assisted Seed Growth Method. *J. Phys. Chem. C* **2013**, *117*, 8916–8923.

18. Hastings, S. P.; Swanglap, P.; Qian, Z.; Fang, Y.; Park, S.-J.; Link, S.; Engheta, N.; Fakhraai, Z. Quadrupole-Enhanced Raman Scattering (QERS). *ACS Nano* **2014**, *8*, 9025–9034.

19. Murphy, C. J.; Thompson, L. B.; Alkilany, A. M.; Sisco, P. N.; Boulos, S. P.; Sivapalan, S. T.; Yang, J. A.; Chernak, D. J.; Huang, J. The Many Faces of Gold Nanorods. *J. Phys. Chem. Lett.* **2010**, *1*, 2867–2875.

20. Njoki, P. N.; Lim, I. I. S.; Mott, D.; Park, H.-Y.; Khan, B.; Mishra, S.; Sujakumar, R.; Luo, J.; Zhong, C.-J. Size Correlation of Optical and Spectroscopic Properties for Gold Nanoparticles. *J. Phys. Chem. C* **2007**, *111*, 14664–14669.

21. Sun, Y.; Xia, Y. Increased Sensitivity of Surface Plasmon Resonance of Gold Nanoshells Compared to That of Gold Solid Colloids in Response to Environmental Changes. *Anal. Chem.* **2002**, *74*, 5297–5305.

22. Shipway, A. N.; Lahav, M.; Gabai, R.; Willner, I. Investigations into the Electrostatically Induced Aggregation of Au Nanoparticles. *Langmuir* **2000**, *16*, 8789–8795.

23. Kelly, K. L.; Coronado, E.; Zhao, L. L.; Schatz, G. C. The Optical Properties of Metal Nanoparticles: the Influence of Size, Shape, and Dielectric Environment. *J. Phys. Chem. B* **2002**, *107*, 668–677.

24. Tsang, L.; Kong, J. A.; Ding, K.-H. *Scattering of Electromagnetic Waves, Theories and Applications*; John Wiley & Sons, Inc., 2000.

25. Alù, A.; Salandrino, A.; Engheta, N. Negative Effective Permeability and Left-Handed Materials at Optical Frequencies. *Opt. Express* **2006**, *14*, 1557–1567.

26. Alù, A.; Engheta, N. Dynamical Theory of Artificial Optical Magnetism Produced by Rings of Plasmonic Nanoparticles. *Phys. Rev. B* **2008**, *78*, 085112.

27. Mühlig, S.; Rockstuhl, C.; Yannopapas, V.; Bürgi, T.; Shalkevich, N.; Lederer, F. Optical Properties of a Fabricated Self-Assembled Bottom-Up Bulk Metamaterial. *Opt. Express* **2011**, *19*, 9607–9616.

28. Bohren, C. F.; Huffman, D. R. *Absorption and Scattering of Light by Small Particles*; Wiley-VCH Verlag GmbH & Co. KGaA: Weinheim, 2004.

29. Sanchez-Gaytan, B. L.; Park, S.-J. Spiky Gold Nanoshells. *Langmuir* **2010**, *26*, 19170–19174.